RSC Advances

ROYAL SOCIETY OF CHEMISTRY

www.rsc.org/advances

Nb-doped VO_x/CeO_2 catalyst for NH_3-SCR of NO_x at low temperatures

Zhihua Lian, Fudong Liu[*†], Hong He[*], Kuo Liu

State Key Joint Laboratory of Environment Simulation and Pollution Control, Research Center for Eco-Environmental Sciences, Chinese Academy of Sciences, Beijing 100085, PR China

[*]Corresponding author. Fax: +86 10 62849123; Tel: +86 10 62849123; E-mail: fudongliu@lbl.gov, lfd1982@gmail.com (F. Liu); honghe@rcees.ac.cn (H. He)

[†] Present address: Materials Sciences Division, Lawrence Berkeley National Laboratory, 1 Cyclotron Road, Berkeley, CA 94720, United States

Abstract

The promotion effect of Nb addition to VO_x/CeO_2 catalyst for the selective catalytic reduction of NO_x by NH_3 was fully investigated. VO_x/CeO_2 and NbO_x doped VO_x/CeO_2 catalysts were characterized by N_2 physisorption, XRD, H_2-TPR and NH_3-TPD. The results showed that the addition of Nb could significantly promote the SCR activity of the VO_x/CeO_2 catalyst, especially in the low temperature range. VO_x/CeO_2 with 30 wt.% NbO_x catalyst showed the best catalytic performance and better SO_2/H_2O tolerance than VO_x/CeO_2 catalyst. 30Nb-1VO_x/CeO_2 also exhibited higher NH_3-SCR activity than $3V_2O_5$-WO_3/TiO_2. The lower crystallinity, the stronger redox capability and the more Brønsted acid sites of the Nb-VO_x/CeO_2 catalyst were all responsible for the more excellent NH_3-SCR performance. Based on kinetic experiments and *in situ* DRIFTS results, it was concluded that the Langmuir-Hinshelwood mechanism existed for selective catalytic reduction of NO over Nb-VO_x/CeO_2, in which adsorbed NO_x species reacted with adsorbed NH_3 to finally form N_2 and H_2O.

Keywords

Selective catalytic reduction of NO_x with NH_3; Low temperature activity; Vanadium-cerium catalyst; Niobium oxide

1 Introduction

Nitrogen oxides (NO and NO_2), which result from automobile exhaust gas and industrial combustion of fossil fuels, have been major pollutants for air pollution. [1] They contribute to a variety of environmentally harmful effects such as photochemical smog, acid rain, and haze formation. [2] The selective catalytic reduction of NO_x with NH_3 (NH_3-SCR) in the presence of excess oxygen is now the most efficient technology for the removal of nitrogen oxides from stationary sources. [2, 3] V_2O_5-WO_3(MoO_3)/TiO_2 has been widely applied as an industrial catalyst for several decades. [4, 5] However, some problems still remain for V_2O_5-WO_3(MoO_3)/TiO_2, such as the relatively narrow operating temperature window of 300-400 ^oC, low N_2 selectivity and high conversion of SO_2 to SO_3 at high temperatures. [4, 6, 7] Besides, the high concentration of ash containing K_2O, CaO, As_2O_3 in the flue gas reduces the performance and longevity of V_2O_5-WO_3(MoO_3)/TiO_2 catalysts. [8, 9] These could be avoided by locating the SCR unit downstream of the electrostatic precipitator unit and even downstream of the desulfurizer, through the development of a highly efficient low temperature SCR system.

In our previous study, we have developed a VO_x/CeO_2 catalyst, prepared by a homogeneous precipitation method, showing excellent NH_3-SCR activity, N_2 selectivity and SO_2 durability. [10] However, the catalytic activity was not high enough for the application in the deNO_x process of exhaust gas with low temperature, such as the flue gas after dust removal and desulfurization from coal-fired power plants.

Therefore, it is very necessary to modify this vanadium-cerium catalyst to improve the low temperature activity, which is crucial for its practical utilization.

Niobium compound materials are of current interest as important catalysts for various reactions, such as the removal of nitrogen oxides, the hydrogenation and oxidative dehydrogenation of alkanes, acting as a catalyst promoter, catalyst support or solid acid catalyst. [11] It was reported that when the niobium oxides were introduced into V_2O_5/TiO_2 catalysts, the conversion of NO in NH_3-SCR reaction increased 2-4 times at low temperatures. [12] The addition of Nb to MnO_x-CeO_2 was also found to be very effective in improving the NH_3-SCR activity and N_2 selectivity. [13, 14] $Mn_2Nb_1O_x$ catalyst exhibited higher NH_3-SCR activity than MnO_x catalyst. [15] In addition, it was reported that the introduction of the third main group element (such as Mn, Fe, Co, Mo) could also improve the activity, stability or SO_2 durability of the SCR catalysts. [16-19] Therefore, based on our V-Ce catalyst, we can add other elements to adjust its physicochemical properties, expecting to enhance the low temperature SCR activity.

In this study, a series of M-VO_x/CeO_2 catalysts (M = Mn, Fe, Co, Nb, Mo) were prepared by the homogeneous precipitation method and were applied to the low-temperature NH_3-SCR reaction. The addition of Nb could significantly promote the SCR activity over the VO_x/CeO_2 catalyst. Among the catalysts with different NbO_x contents, VO_x/CeO_2 with 30 wt.% NbO_x catalyst showed the best catalytic performance and better SO_2/H_2O tolerance compared to VO_x/CeO_2 catalyst. The lower crystallinity, the stronger redox capability and the more Brønsted acid sites of the Nb-VO_x/CeO_2 catalyst were all responsible for its higher SCR activity.

2 Experiments

2.1 Catalyst synthesis and activity tests

The VO_x/CeO_2 oxide catalysts were prepared by a homogeneous precipitation method. Aqueous solutions of NH_4VO_3 ($H_2C_2O_4$ was added to facilitate the dissolution of NH_4VO_3) and $Ce(NO_3)_2$ were mixed with the desired molar ratios (the mass ratio of vanadium oxide was controlled at 1 wt.%). An excess of aqueous urea solution was then added to the mixed solution. The solution was heated to 90 ℃ and held there for 12 h under vigorous stirring. After filtration and washing with deionized water, the resulting precipitate was dried at 100 ℃ overnight and subsequently calcined at 350 ^oC for 3 h in air. M-VO_x/CeO_2 catalysts (the mass ratio of MO_x were controlled at 30 wt.%) were also prepared by homogeneous precipitation methods using $Mn(NO_3)_2$, $Co(NO_3)_3$, $Fe(NO_3)_3$, $NbCl_5$, and $(NH_4)_6Mo_7O_{24}$ as precursors, respectively. Nb-VO_x/CeO_2 catalysts with different Nb contents (10, 30, 50 wt.%) and the unpromoted 3 wt.% VO_x/CeO_2 catalyst were also prepared by the same method. For comparison, the conventional 3 wt.% V_2O_5-10 wt.% WO_3/TiO_2 and 1 wt.% V_2O_5-10 wt.% WO_3/TiO_2 were prepared by impregnation method using NH_4VO_3, $(NH_4)_{10}W_{12}O_{41}$, $H_2C_2O_4\,2H_2O$ as precursors and anatase TiO_2 as support. After impregnation, the excess water was removed in a rotary evaporator at 60 ^oC. The samples dried at 100 ^oC overnight and then calcined at 500 ^oC for 3h in air condition.

Before NH_3-SCR activity tests, the catalysts were pressed, crushed and sieved to 40-60 mesh. The SCR activity tests were carried out in a fixed-bed quartz flow reactor

at atmospheric pressure. The reaction conditions were controlled as follows: 500 ppm NO, 500 ppm NH_3, 5 vol.% O_2, 100 ppm SO_2 (when used), N_2 balance. Under ambient conditions, the total flow rate was 500 ml/min and the gas hourly space velocity (GHSV) was 50 000 h^{-1}. The amount of catalysts used in activity tests was 0.6 ml (about 0.7 g). The effluent gas including NO, NH_3, NO_2 and N_2O was continuously analyzed by an FTIR spectrometer (Nicole Nexus 670) equipped with a heated, low-volume multiple-path gas cell (2m). The FTIR spectra were collected after the SCR reaction reached a steady state, and the NO_x conversion and N_2 selectivity were calculated as follows:

$$NO_x conversion = \left(1 - \frac{[NO]_{out} + [NO_2]_{out}}{[NO]_{in} + [NO_2]_{in}}\right) \times 100\%$$

$$N_2 selectivity = \frac{[NO]_{in} + [NH_3]_{in} - [NO_2]_{out} - 2[N_2O]_{out}}{[NO]_{in} + [NH_3]_{in}} \times 100\%$$

2.2 Characterization of catalysts

The surface area and pore characterization of the catalysts were obtained from N_2 adsorption/desorption analysis at -196 ℃ using a Quantachrome Quadrasorb SI-MP. Prior to the N_2 physisorption, the catalysts were degassed at 300 ^oC for 5 h. Surface areas were determined by the BET equation in the 0.05-0.35 partial pressure range. Pore volumes and average pore diameters were determined by the Barrett-Joyner-Halenda (BJH) method from the desorption branches of the isotherms.

Powder X-ray diffraction (XRD) measurements of the catalysts were carried out on a computerized PANalytical X'Pert Pro diffractometer with Cu Kα (λ = 0.15406 nm)

radiation. The data of 2θ from 10 to 80^{o} were collected at 8^{o}/min with the step size of 0.07^{o}.

The H_2-TPR experiments were carried out on a Micromeritics Auto Chem 2920 chemisorption analyzer. The samples (30 mg) were pretreated at 300 ^{o}C in a flow of 20 vol.% O_2/Ar (50 ml/min) for 0.5 h in a quartz reactor and cooled down to room temperature (30 ^{o}C) followed by Ar purging for 0.5 h. A 50 mL/min gas flow of 10% H_2 in Ar was then passed over the samples through a cold trap to the detector. The reduction temperature was raised at 10 ^{o}C min^{-1} from 30 to 1000 ^{o}C.

2.3 NH_3-TPD studies

NH_3-TPD experiments were performed in the same instrument as the H_2-TPR, equipped with a quadrupole mass spectrometer (MKS Cirrus) to record the signals of NH_3 (m/z = 17 for NH_3, the interference of H_2O was eliminated by using a cold trap before the detector). Prior to TPD experiments, the samples (100 mg) were pretreated at 300 ^{o}C in a flow of 20 vol.% O_2/Ar (50 ml/min) for 0.5 h and cooled down to room temperature (30 ^{o}C). The samples were then exposed to a flow of 2500 ppm NH_3/Ar (50 ml/min) at 30 ^{o}C for 1 h, followed by Ar purging for another 1 h. Finally, the temperature was raised to 600 ^{o}C in Ar flow at the rate of 10 ^{o}C min^{-1}.

2.4 *In situ* DRIFTS studies

In situ DRIFTS experiments were performed on an FTIR spectrometer (Nicolet Nexus 670) equipped with a smart collector and an MCT/A detector cooled by liquid nitrogen. The reaction temperature was controlled precisely by an Omega

programmable temperature controller. Prior to each experiment, the sample was pretreated at 300 ^{o}C for 0.5 h in a flow of 20 vol.% O_2/N_2 and then cooled down to 175 ^{o}C. The background spectra were collected in flowing N_2 and automatically subtracted from the sample spectrum. The reaction conditions were controlled as follows: 200 ml/min total flow rate, 500 ppm NH_3 or/and 500 ppm NO + 5 vol.% O_2, and N_2 balance. All spectra were recorded by accumulating 100 scans with a resolution of 4 cm^{-1}.

3 Results and Discussion

3.1 Catalytic performance

3.1.1 SCR activity over 30M-1VO_x/CeO_2

Fig. 1 shows the NO_x conversion and N_2 selectivity over VO_x/CeO_2 and doped VO_x/CeO_2 catalysts. The VO_x/CeO_2 catalyst presented 80% NO_x conversion at 200 ^{o}C. Mn doped VO_x/CeO_2 exhibited nearly 100% NO_x conversion at 100-200 ^{o}C, but the NO_x conversion decreased rapidly above 200 ^{o}C. It also showed lower N_2 selectivity in the whole temperature that we investigated. NH_3-SCR activities over Fe, Co and Mo doped VO_x/CeO_2 catalysts were all lower than that over VO_x/CeO_2. Among these catalysts, Co doped VO_x/CeO_2 catalyst presented the lowest NO_x conversion and the maximal NO_x conversion was only 50%. Furthermore, the N_2 selectivity over Co-VO_x/CeO_2 was rather low. Contrarily, Nb doped VO_x/CeO_2 catalyst exhibited higher catalytic performance than the VO_x/CeO_2 catalyst. The addition of Nb enhanced the NO_x conversion and N_2 selectivity over VO_x/CeO_2 simultaneously. It

showed 60% and 90% NO_x conversion at 150 and 175 ^oC, respectively, and 100% N_2 selectivity was obtained in the temperature range of 100-350 ^oC. The best NH_3-SCR activity was obtained over the Nb doped VO_x/CeO_2 catalyst, therefore we chose Nb to further investigate the influence of doping amount on the catalyst structure and catalytic performance.

3.1.2 SCR activity over Nb-1VO_x/CeO_2 catalysts

The effect of NbO_x addition amount to VO_x/CeO_2 catalyst on NO_x conversion was shown in Fig. 2. 10 wt.% NbO_x doped VO_x/CeO_2 catalyst showed higher NH_3-SCR activity than unpromoted VO_x/CeO_2 catalyst. The 30Nb-VO_x/CeO_2 catalyst presented the best catalytic activity, over which NO_x was completely reduced at about 175 ^oC. Any further increase in Nb content resulted in a decline in activity. These indicated that Nb content had a significant effect on the SCR activity over VO_x/CeO_2 catalysts, and 30 wt.% NbO_x was optimal. Although, for the 30Nb-VO_x/CeO_2 catalyst, the content of 1% V seems to be negligible comparing with 30% Nb, V indeed played an important role in NH_3-SCR reaction and 30Nb-VO_x/CeO_2 exhibited much higher catalytic activity than 30Nb/CeO_2 (as shown in Fig. S1). At lower than 175 ^oC, the reaction rates normalized by surface area over 30Nb-VO_x/CeO_2 was higher than that over VO_x/CeO_2 (as shown in Fig. S2). The highest reaction rate over 30Nb-VO_x/CeO_2 was obtained at 175-350 ^oC. The lower reaction rates over 30Nb-VO_x/CeO_2 than VO_x/CeO_2 above 200 ^oC were due to its larger specific surface area and similar NO_x conversion. 30Nb-1VO_x/CeO_2 and 1VO_x/CeO_2 catalyst were chosen as the model catalysts to carry out further investigation, such as the effect of Nb on H_2O/SO_2

tolerance and the relationship between catalyst structure and catalytic activity.

To better evaluate the NH_3-SCR activity over Nb-VO_x/CeO_2 catalyst, we also carried out the comparative SCR activity test over V_2O_5-WO_3/TiO_2 (Fig. 3). 30 wt.% Nb-$1VO_x/CeO_2$ exhibited higher NO_x conversion than $1VO_x/CeO_2$ and $3VO_x/CeO_2$. However, there was not notable enhancement over 30Nb-$3VO_x/CeO_2$ in contrast to $3VO_x/CeO_2$ (as shown in Fig. S3). Compared to $3VO_x/CeO_2$, the 30Nb-$1VO_x/CeO_2$ catalyst not only decreased the content of vanadium oxide, but also enhanced the catalytic activity. The NH_3-SCR performance over 30Nb-$1VO_x/CeO_2$ catalyst was also better than that over $3V_2O_5$-$10WO_3/TiO_2$ and $1V_2O_5$-$10WO_3/TiO_2$. The NO_x conversion over three catalysts at 175 ^oC was 96%, 63% and 15%, respectively. Therefore, 30Nb-$1VO_x/CeO_2$ showed excellent NH_3-SCR performance.

3.1.3 Influence of H_2O and SO_2 on SCR activity

Fig. 4 shows the effect of SO_2 and H_2O on the catalytic activity over $1VO_x/CeO_2$ and 30Nb-$1VO_x/CeO_2$ catalysts at 250 ^oC. When 100 ppm SO_2 was introduced to the inlet gas, the NO_x conversion over VO_x/CeO_2 decreased to 24% in 48 h and could not recover to the initial activity after the removal of SO_2, which indicates that the inhibiting effect of SO_2 on the SCR activity over the VO_x/CeO_2 catalyst was severe and irreversible. However, the SO_2 inhibiting effect over Nb-VO_x/CeO_2 was quite different. The NO_x conversion decreased slightly, and nearly 90% NO_x conversion was obtained in the presence of 100 ppm SO_2 for a 48 h test. The NH_3-SCR performance over VO_x/CeO_2 catalysts after SO_2 poisoning for 48 h is shown in Fig.

S4. The activity over Nb-VO_x/CeO_2 was still higher than that over VO_x/CeO_2. 95% NO_x conversion could be obtained on the Nb-VO_x/CeO_2 catalyst at 250 ^oC and only 26% NO_x conversion on VO_x/CeO_2. This proved again that the Nb-VO_x/CeO_2 catalyst showed higher SO_2 resistance than VO_x/CeO_2.

When 5% H_2O was introduced to the inlet gas, the NO_x conversion over VO_x/CeO_2 decreased rapidly to 56% and kept in 56% in 48 h test. The catalytic activity could recover to the original level after the removal of H_2O, indicating that the poison of H_2O was reversible. Meanwhile, H_2O had no influence on the catalytic activity over Nb-VO_x/CeO_2 catalyst and 100% NO_x conversion was maintained all the time. Nb-VO_x/CeO_2 exhibited much higher catalytic activity and stronger resistance to SO_2/H_2O than VO_x/CeO_2.

3.2 Catalyst Characterization

3.2.1 N_2 physisorption

Table 1 shows the N_2 physisorption results of $1VO_x/CeO_2$ and 30Nb-$1VO_x/CeO_2$ catalysts. Nb-VO_x/CeO_2 catalyst presented larger specific surface area and pore volume than VO_x/CeO_2. The addition of Nb to VO_x/CeO_2 resulted in bigger specific surface area and pore volume, which is beneficial to the enhancement of SCR activity.

3.2.2 XRD

The XRD patterns of $1VO_x/CeO_2$ and 30Nb-$1VO_x/CeO_2$ catalysts are shown in Fig. 5. For both catalysts, all the peaks in the diffraction profiles attributed to CeO_2 of a cubic fluorite structure (43-1002). No vanadium species and niobium species were

detected, suggesting that V and Nb species were highly dispersed on the catalysts. The intensity of peaks of Nb doped catalyst was weaker than that of VO_x/CeO_2, indicating a loss of crystallinity. The deceasing crystallinity may contribute to the increase of surface area.

3.2.3 H_2-TPR

The redox properties of $1VO_x/CeO_2$ and $30Nb\text{-}1VO_x/CeO_2$ catalysts were investigated by H_2-TPR and the spectra are shown in Fig. 6. There are three peaks at 380, 460 and 710 ^oC (740 ^oC) over $1VO_x/CeO_2$ and $30Nb\text{-}1VO_x/CeO_2$. According to the literatures [10, 20], the reduction peaks of surface Ce^{4+} to Ce^{3+} and the bulk Ce^{4+} to Ce^{3+} were centered at 509 and 812 ^oC, respectively. The reduction peaks at 399, 523 and 766 ^oC over CeO_2 could be assigned to the reduction of surface oxygen species, that of oxygen in deeper interior and that of oxygen in bulk, respectively. [21] The reduction peak around 400-500 ^oC is due to the surface vanadium oxide, while high temperature peak over 700 ^oC is assigned to the reduction of bulk vanadium oxide. [22] Niobium oxide could be reduced at much higher temperature. [15] Therefore, the low temperature peak at 380 ^oC and 460 ^oC could be due to the reduction of surface Ce^{4+} and V^{5+} and that in deeper interior, respectively. The TPR peak at 710 ^oC (740 ^oC) could be attributed to the reduction of bulk Ce and V. Both V and Ce possessed redox capability and acted as reactive sites to catalyze NH_3-SCR reaction. The amount of H_2 consumption of $Nb\text{-}VO_x/CeO_2$ catalyst was higher than that of VO_x/CeO_2 (1.15:1). The intensity of the low temperature (380 ^oC) reduction peak of $Nb\text{-}VO_x/CeO_2$ was much stronger than that of VO_x/CeO_2 (1.44:1). This could be due to the interaction of

V, Ce and Nb over Nb-VO_x/CeO_2 catalyst resulting in better dispersion of vanadium species and stronger redox capability. The active temperature window in NH_3-SCR reaction was between 150-400 ^oC. Stronger redox capability in this temperature range could enhance NH_3-SCR performance. Therefore, Nb doped VO_x/CeO_2 showed higher NH_3-SCR activity.

3.2.4 NH_3-TPD

Fig. 7 shows NH_3-TPD results over $1VO_x/CeO_2$ and $30Nb\text{-}1VO_x/CeO_2$ catalysts using the fragment of m/z = 17 to identify NH_3. There were two NH_3 desorption peaks around 100 and 250 ^oC on both catalysts. It is generally accepted that NH_4^+ ions bound to Brønsted acid sites are less thermally stable than coordinated NH_3 molecules bound to Lewis acid sites and desorb at lower temperatures. [18, 23, 24] Therefore, the desorption peak at 100 ^oC could be ascribed to the desorption of physisorbed NH_3 and the partial ionic NH_4^+ bound to the weak Brønsted acid sites, and the peak at 250 ^oC could be assigned to the desorption of ionic NH_4^+ bound to strong Brønsted acid sites and coordinated NH_3 bound to the Lewis acid sites. The amount of acid sites over Nb-VO_x/CeO_2 was remarkably larger than that of VO_x/CeO_2 (1.68:1). It indicates that Nb-VO_x/CeO_2 catalyst presented more acid sites which could facilitate the adsorption and activation of NH_3 during catalytic reaction even in the presence of H_2O and SO_2 thus enhances the catalytic activity in NH_3-SCR. In the presence of SO_2, more acid sites over Nb-VO_x/CeO_2 catalyst inhibited the adsorption of SO_2 and the deposition of sulfate thus enhanced the resistance to SO_2. More acid sites could also promote the adsorption of NH_3 in the presence of H_2O and weaken the competitive adsorption of

H_2O with NH_3. Furthermore, larger specific surface area was obtained over Nb-VO_x/CeO_2. Therefore, Nb-VO_x/CeO_2 catalyst showed stronger resistance to H_2O/SO_2.

3.3 *In situ* DRIFTS studies

To investigate NH_3/NO_x adsorption on 1VO_x/CeO_2 and 30Nb-1VO_x/CeO_2 catalysts together with the SCR reaction mechanism, *in situ* DRIFTS were conducted at 175 ^oC and the results of NH_3 adsorption on VO_x/CeO_2 and Nb-VO_x/CeO_2 catalysts are shown in Fig. 8A. After NH_3 adsorption and N_2 purge, both catalysts were covered by different NH_3 species. The bands at 1423 and 1670 cm^{-1} were assigned to asymmetric and symmetric bending vibrations of ionic NH_4^+ on Brønsted acid sites and the bands at 1596 (1604) and 1147 (1200) cm^{-1} were attributed to asymmetric and symmetric bending vibrations of the N-H bonds in NH_3 coordinately linked to the Lewis acid sites. [25-27] Nb-VO_x/CeO_2 catalyst provided more acid sites than VO_x/CeO_2 (1.71:1), especially the Brønsted acid sites, than VO_x/CeO_2, which was in well harmony with the NH_3-TPD results. As shown in our previous paper (Chemical Engineering Journal 250 (2014) 390-398)[15], the NbO_x itself did not show any NH_3-SCR activity in the whole temperature range that we investigated. However, the addition of Nb to 1VO_x/CeO_2 increased the surface acidity. Nb mainly played as acid sites for the promotion of NH_3 adsorption in NH_3-SCR reaction.

The *in situ* DRIFT spectra of NO + O_2 adsorption on 1VO_x/CeO_2 and 30Nb-1VO_x/CeO_2 catalysts at 175 ^oC were also conducted, and the results are shown

in Fig. 8B. When VO_x/CeO_2 catalyst was exposed to NO + O_2, bands assigned to nitrate species were observed including monodentate nitrate (1540 and 1270 cm^{-1}), bridging nitrate (1215 and 1592 cm^{-1}) and bidentate nitrate (1570 and 1243 cm^{-1}). [28-30] On the Nb-VO_x/CeO_2 catalyst, the adsorption amount of NO_x was larger than that on the VO_x/CeO_2 catalyst (1.67:1). The addition of Nb to the VO_x/CeO_2 catalyst increased the acidity but did not inhibit the adsorption of NO_x on the catalyst surface simultaneously. It could be due to its stronger oxidation at low temperature and its larger specific surface area. Therefore, the Nb-VO_x/CeO_2 catalyst produced more nitrate species than VO_x/CeO_2.

According to the Arrhenius equation, the activation energy over VO_x/CeO_2 and Nb-VO_x/CeO_2 catalysts was calculated as 47 and 38 kJ/mol (as shown in Fig. S5). The interaction of V, Ce and Nb of the Nb-VO_x/CeO_2 catalyst decreased the activation energy of NO reduction and promote the NH_3-SCR reaction.

To investigate the reactivity of adsorbed NH_3 species in the SCR reaction on 30Nb-1VO_x/CeO_2 catalysts, the *in situ* DRIFTS of reaction between pre-adsorbed NH_3 and NO + O_2 at 175 ^oC were recorded as a function of time (Fig. 9A). After NH_3 pre-adsorption and N_2 purge, the catalyst surface was covered by the adsorbed NH_3 species. When NO + O_2 was introduced, the intensity of the bands attributed to NH_3 species decreased and disappeared after 10 min. At the same time, the bands assigned to nitrate species (monodentate nitrate at 1540 cm^{-1}, bridging nitrate at 1215, 1592 cm^{-1} and bidentate nitrate at 1570, 1243 cm^{-1}) appeared. This result suggested that both ionic NH_4^+ and coordinated NH_3 could react with NO_x and participate in the

307 NH_3-SCR reactions. Fig. S6 showed the band intensities of adsorbed NH_3 species
308 over VO_x/CeO_2 and 30Nb-VO_x/CeO_2 pretreated by exposure to NH_3 followed by
309 exposure to NO + O_2 at 175 ^oC. The reactive rate of adsorbed NH_3 species with gas
310 NO and O_2 over Nb-VO_x/CeO_2 was much higher than that over VO_x/CeO_2. Therefore,
311 more adsorbed NH_3 species on Nb-VO_x/CeO_2 contributed to its better SCR activity.

312 The reaction between the pre-adsorbed NO_x and NH_3 on 30Nb-1VO_x/CeO_2
313 catalysts was also investigated by the *in situ* DRIFTS, and the results were shown in
314 Fig. 9B. After NO + O_2 pre-adsorption and N_2 purge, Nb-VO_x/CeO_2 catalyst surface
315 was covered by various nitrate species. When NH_3 was introduced, the intensity of
316 bridging nitrate decreased, which indicated that adsorbed NO_x species could also react
317 with NH_3. NH_3 adsorbed species were observed at the band of 1427 cm^{-1}.

318 The kinetic experiments were also carried out to investigate the reaction order and
319 the tests met the condition of differential reactor model. The NO conversion data in
320 the kinetics test were in differential regime (conversion less than 20%) (as shown in
321 Fig. S7). A relative small particles size (40-60 mesh) and the volume hourly space
322 velocity (about 500 000 h^{-1}) [31] ensured the elimination of internal and external
323 diffusion, respectively. The rates of NO conversion increased linearly with NO
324 concentration over 30Nb-1VO_x/CeO_2 catalyst (as shown in Fig. S8), and the reaction
325 order for NO was calculated as 0.555. The reaction order for NO was lower than 1,
326 indicating the presence of Langmuir-Hinshelwood mechanism, which was in
327 agreement with DRIFTS results. In Fig. 9B, the intensity of the bands attributed to
328 nitrate species weakened after exposure to NH_3 indicating that adsorbed NO_x species

could react with adsorbed NH_3 to finally form N_2 and H_2O. In our previous study [10], for the $3VO_x/CeO_2$ catalysts pre-adsorbed NO_x species, when NH_3 was introduced, the intensity of the bands attributed to monodentate nitrate and bridging nitrate species decreased slightly. The amount of bidentate nitrate species increased markedly, which may be due to the transformation of monodentate and bridging nitrate to bidentate nitrate (Fig. 10 [10] and Fig. S5 [10]). The adsorbed nitrate species were mostly inactive in the NH_3-SCR reaction and therefore the $3VO_x/CeO_2$ catalysts mainly followed the Eley-Rideal mechanism.

4 Conclusions

A systematic study on the effect of Nb addition to the VO_x/CeO_2 catalyst for the low-temperature NH_3-SCR reaction was carried out. VO_x/CeO_2 and Nb doped VO_x/CeO_2 catalysts were prepared by homogeneous precipitation method and the SCR activity at low temperature was enhanced by the addition of Nb. The NH_3-SCR activity over $1\%VO_x/CeO_2$ with 30 wt.% NbO_x catalyst were higher than that over the $3\%V_2O_5$-WO_3/CeO_2 catalyst. $30Nb\text{-}1VO_x/CeO_2$ showed higher catalytic activity than $1VO_x/CeO_2$ catalyst, due to the weaker crystallinity, the stronger redox capability and the more Brønsted acid sites. The excellent SO_2/H_2O tolerance was also obtained over $30Nb\text{-}1VO_x/CeO_2$ catalyst. The Langmuir-Hinshelwood mechanism existed for selective catalytic reduction of NO Over $30Nb\text{-}1VO_x/CeO_2$, in which adsorbed NO_x species reacted with adsorbed NH_3 to finally form N_2 and H_2O.

Acknowledgements

This work was financially supported by the National Natural Science Foundation of China (51108446, 51221892) and the Ministry of Science and Technology, China (2013AA065301, 2012AA062506).

Reference

1. G. S. Qi, R. T. Yang and R. Chang, *Appl. Catal. B-environ.*, 2004, **51**, 93.
2. H. Bosch, and Janssen, F., *Catal. Today*, 1988, **2**, 369.
3. Z. G. Huang, Z. P. Zhu, Z. Y. Liu and Q. Y. Liu, *J. Catal.*, 2003, **214**, 213.
4. G. Busca, L. Lietti, G. Ramis and F. Berti, *Appl. Catal. B-environ.*, 1998, **18**, 1.
5. G. Busca, M. A. Larrubia, L. Arrighi and G. Ramis, *Catal. Today.*, 2005, **107-108**, 139.
6. J. P.Dunn, P. R.Koppula, H. G.Stenger and I. E.Wachs, *Appl. Catal. B-environ.*, 1998, **19**, 103.
7. P. Balle, B. Geiger and S. Kureti, *Appl. Catal. B-environ.*, 2009, **85**, 109.
8. I. E. Wachs and B. M. Weckhuysen, *Appl. Catal. A-gen.*, 1997, **157**, 67.
9. D. A. Bulushev, F. Rainone, L. Kiwi-Minsker and A. Renken, *Langmuir*, 2001, **17**, 5276.
10. Z. Lian, F. Liu and H. He, *Catal. Sci. Technol.*, 2015, **5**, 389.
11. K. Tanabe, *Catal. Today.*, 2003, **78**, 65.
12. K.A.Vikulov, A.Andreini, E.K.Poels and A.Bliek, *Catal. Lett.*, 1994, **25**, 49.
13. M. Casapu, O. Krocher, M. Mehring, M. Nachtegaal, C. Borca, M. Harfouche and D. Grolimund, *J. Phys. Chem. C.*, 2010, **114**, 9791.
14. M. Casapu, O. Kröcher and M. Elsener, *Appl. Catal. B-environ.*, 2009, **88**, 413.
15. Z. Lian, F. Liu, H. He, X. Shi, J. Mo and Z. Wu, *Chem. Eng. J.*, 2014, **250**, 390.
16. F. Liu, H. He, Y. Ding and C. Zhang, *Appl. Catal. B-environ.*, 2009, **93**, 194.
17. X. Li and Y. Li, *J. Mol. Catal. A-chem.*, 2014, **386**, 69.
18. Sounak Roy, B.Viswanath, M.S.Hedge and G. Madras, *J. Phys. Chem. C*, 2008, **112**, 6002.
19. Z. Liu, S. Zhang, J. Li and L. Ma, *Appl. Catal. B-environ.*, 2014, **144**, 90.
20. Y. Peng, J. H. Li, L. Chen, J. H. Chen, J. Han, H. Zhang and W. Han, *Environ. Sci. Technol.*, 2012, **46**, 2864.
21. S. J. Yang, Y. F. Guo, H. Z. Chang, L. Ma, Y. Peng, Z. Qu, N. Q. Yan, C. Z. Wang and J. H. Li, *Appl. Catal. B-environ.*, 2013, **136**, 19.
22. S. Youn, S. Jeong and D. H. Kim, *Catal. Today.*, 2014, **232**, 185.
23. R. B. Jin, Y. Liu, Z. B. Wu, H. Q. Wang and T. T. Gu, *Chemosphere*, 2010, **78**, 1160.
24. K. J. Lee, M. S. Maqbool, P. A. Kumar, K. H. Song and H. P. Ha, *Catal. Lett.*, 2013, DOI: 10.1007/s10562-013-1035-1.
25. R. Gao, D. Zhang, X. Liu, L. Shi, P. Maitarad, H. Li, J. Zhang and W. Cao, *Catal. Sci. Technol.*, 2013, **3**, 191.
26. L. Zhang, J. Pierce, V. L. Leung, D. Wang and W. S. Epling, *J. Phys. Chem. C.*, 2013, **117**, 8282.
27. K. J. Lee, P. A. Kumar, M. S. Maqbool, K. N. Rao, K. H. Song and H. P. Ha, *Appl. Catal. B-environ.*, 2013, **142**, 705.
28. K. I. Hadjiivanov, *Catal. Rev. -Sci. Eng.*, 2000, **42**, 71.
29. C. Liu, L. Chen, J. Li, L. Ma, H. Arandiyan, Y. Du, J. Xu and J. Hao, *Environ. Sci. Technol.*, 2012, **46**, 6182.

30. Z. Si, D. Weng, X. Wu, Z. Ma, J. Ma and R. Ran, *Catal. Today.*, 2013, **201**, 122.
31. R. Raj, M. P. Harold and V. Balakotaiah, *Ind. Eng. Chem. Res.*, 2013, **52**, 15455.

394 Table 1 N_2 physisorption of VO_x/CeO_2 and Nb-VO_x/CeO_2 catalysts

Catalysts	Specific surface area (m^2/g)	Pore diameter (nm)	Pore volume (cc/g)
$1VO_x/CeO_2$	131.3	3.50	0.11
$30Nb\text{-}1VO_x/CeO_2$	168.2	3.48	0.15

395

Figure Captions

Fig. 1 The NO_x conversion (A) and N_2 selectivity (B) over M-VO_x/CeO_2 catalysts. Reaction conditions: [NO] = [NH_3] = 500 ppm, [O_2] = 5 vol. %, N_2 balance, total flow rate 500 ml/min and GHSV = 50 000 h^{-1}.

Fig. 2 NH_3-SCR activity over Nb-VO_x/CeO_2 catalysts. Reaction conditions: [NO] = [NH_3] = 500 ppm, [O_2] = 5 vol. %, N_2 balance, total flow rate 500 ml/min and GHSV = 50 000 h^{-1}.

Fig. 3 NH_3-SCR activity over VO_x/CeO_2 and V_2O_5-WO_3/TiO_2 catalysts. Reaction conditions: [NO] = [NH_3] = 500 ppm, [O_2] = 5 vol. %, N_2 balance, total flow rate 500 ml/min and GHSV = 50 000 h^{-1}.

Fig. 4 Effect of SO_2 and H_2O on NH_3-SCR activity over VO_x/CeO_2 and Nb-VO_x/CeO_2 catalysts at 250 ^oC. Reaction conditions: [NO] = [NH_3] = 500 ppm, [SO_2] = 100 ppm (when used), [H_2O] = 5% (when used), [O_2] = 5 vol. %, N_2 balance, total flow rate 500 ml/min and GHSV = 50 000 h^{-1}.

Fig. 5 XRD patterns of VO_x/CeO_2 and Nb-VO_x/CeO_2 catalysts.

Fig. 6 H_2-TPR results over VO_x/CeO_2 and Nb-VO_x/CeO_2 catalysts.

Fig. 7 NH_3-TPD results over VO_x/CeO_2 and Nb-VO_x/CeO_2 catalysts.

Fig. 8 DRIFT spectra of 500 ppm NH_3 adsorption (A) and 500 ppm NO + 5 vol.% O_2 adsorption (B) on VO_x/CeO_2 and Nb-VO_x/CeO_2 catalysts.

Fig. 9 *In situ* DRIFT spectra over Nb-VO_x/CeO_2 pretreated by exposure to NO + O_2 followed by exposure to NH_3 at 175 ^oC (A), and by exposure to NH_3 followed by exposure to NO + O_2 at 175 ^oC (B).

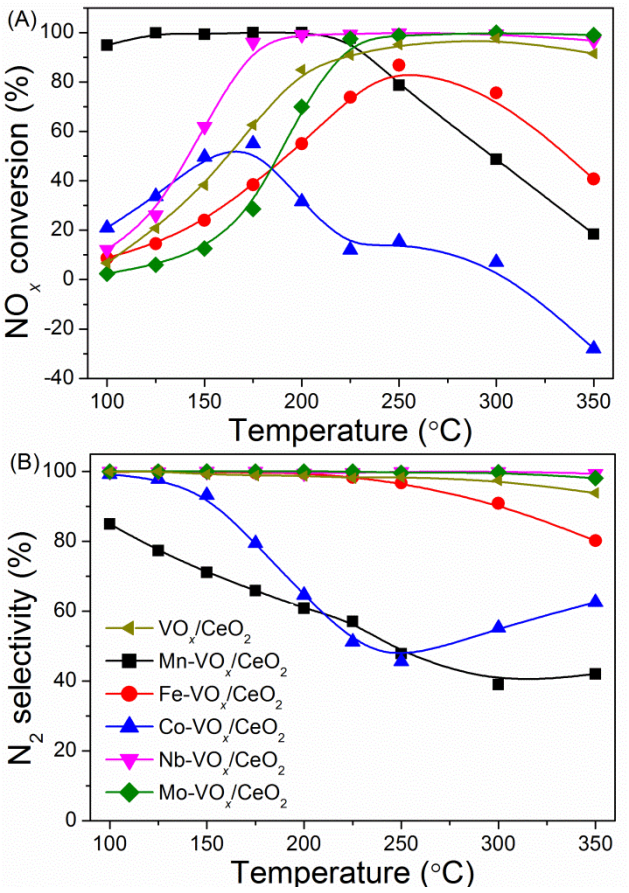

Fig. 1 The NO_x conversion (A) and N_2 selectivity (B) over M-VO_x/CeO_2 catalysts.

Reaction conditions: [NO] = [NH_3] = 500 ppm, [O_2] = 5 vol. %, N_2 balance, total flow rate 500 ml/min and GHSV = 50 000 h^{-1}.

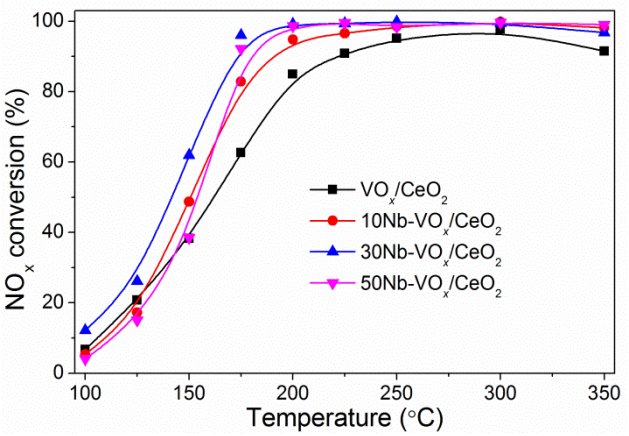

Fig. 2 NH_3-SCR activity over Nb-VO_x/CeO_2 catalysts.

Reaction conditions: [NO] = [NH_3] = 500 ppm, [O_2] = 5 vol. %, N_2 balance, total flow rate 500 ml/min and GHSV = 50 000 h^{-1}.

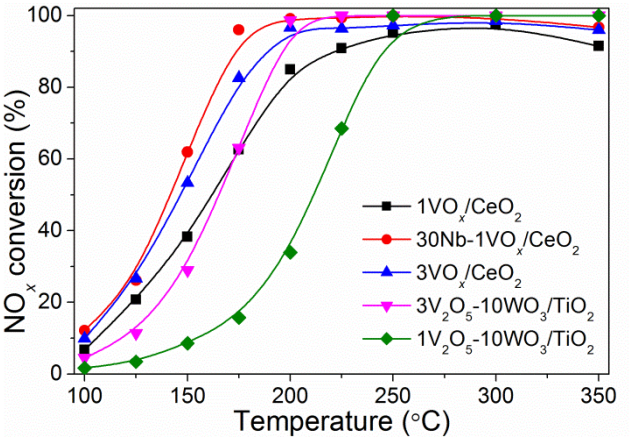

Fig. 3 NH_3-SCR activity over VO_x/CeO_2 and V_2O_5-WO_3/TiO_2 catalysts.

Reaction conditions: [NO] = [NH_3] = 500 ppm, [O_2] = 5 vol. %, N_2 balance, total flow rate 500 ml/min and GHSV = 50 000 h^{-1}.

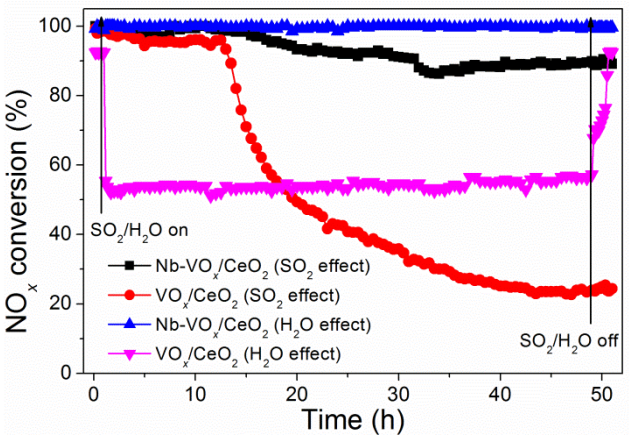

435

436 Fig. 4 Effect of SO_2 and H_2O on NH_3-SCR activity over VO_x/CeO_2 and Nb-VO_x/CeO_2

437 catalysts at 250 ^oC. Reaction conditions: [NO] = [NH_3] = 500 ppm, [SO_2] = 100 ppm

438 (when used), [H_2O] = 5% (when used), [O_2] = 5 vol. %, N_2 balance, total flow rate

439 500 ml/min and GHSV = 50 000 h^{-1}.

440

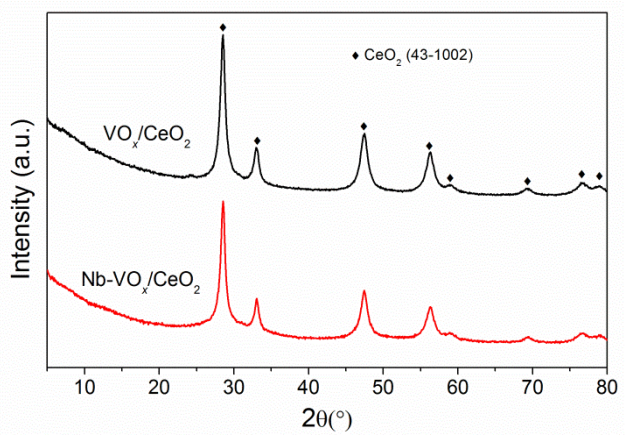

Fig. 5 XRD patterns of VO_x/CeO_2 and Nb-VO_x/CeO_2 catalysts.

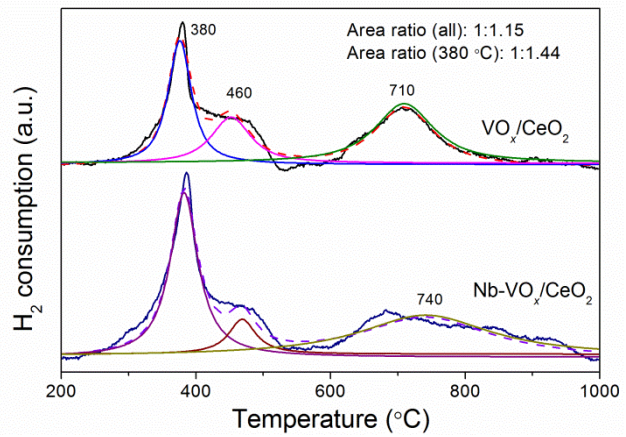

Fig. 6 H_2-TPR results over VO_x/CeO_2 and Nb-VO_x/CeO_2 catalysts.

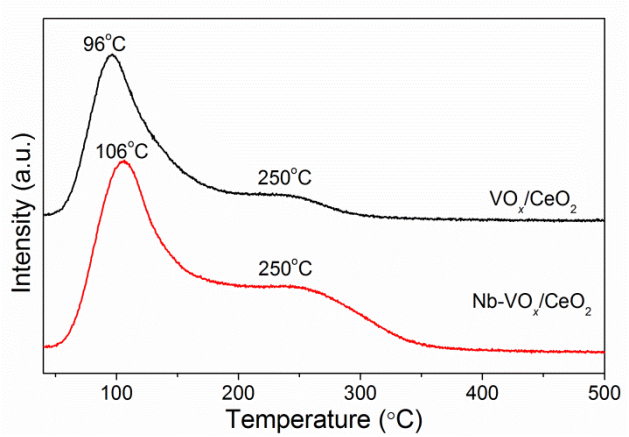

Fig. 7 NH_3-TPD results over VO_x/CeO_2 and Nb-VO_x/CeO_2 catalysts.

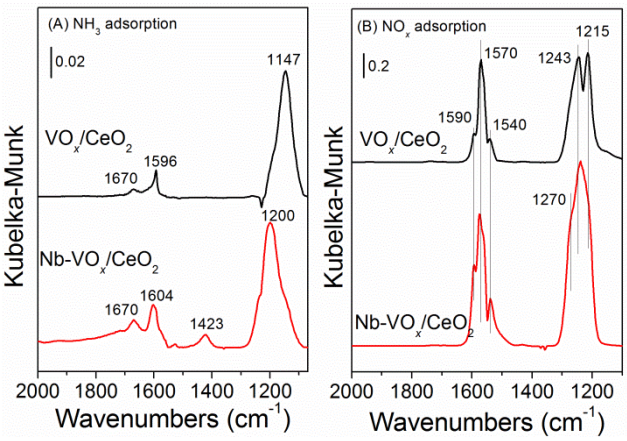

Fig. 8 DRIFT spectra of 500 ppm NH_3 adsorption (A) and 500 ppm NO + 5 vol.% O_2 adsorption (B) on VO_x/CeO_2 and Nb-VO_x/CeO_2 catalysts.

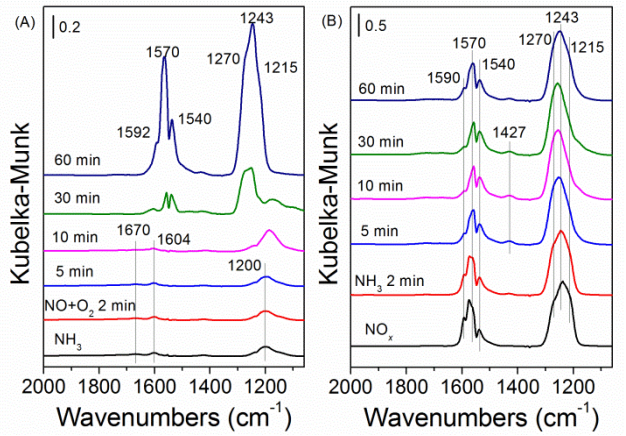

Fig. 9 *In situ* DRIFT spectra over Nb-VO_x/CeO_2 pretreated by exposure to NO + O_2 followed by exposure to NH_3 at 175 ^oC (A), and by exposure to NH_3 followed by exposure to NO + O_2 at 175 ^oC (B).